INTERNATIONAL JOURNAL OF HYDROGEN ENERGY 39 (2014) 9409–9419

Available online at www.sciencedirect.com

ScienceDirect

journal homepage: www.elsevier.com/locate/he

Liquid water breakthrough pressure through gas diffusion layer of proton exchange membrane fuel cell

*Mehdi Mortazavi**, *Kazuya Tajiri*

Mechanical Engineering—Engineering Mechanics, Michigan Technological University, 1400 Townsend Drive, Houghton, MI 49931, USA

ARTICLE INFO

Article history:
Received 15 January 2014
Received in revised form
27 March 2014
Accepted 29 March 2014
Available online 5 May 2014

Keywords:
PEM fuel cell
Gas diffusion layer (GDL)
Breakthrough pressure
Water transport

ABSTRACT

The dynamic behavior of liquid water transport through the gas diffusion layer (GDL) of the proton exchange membrane fuel cell is studied with an ex-situ approach. The liquid water breakthrough pressure is measured in the region between the capillary fingering and the stable displacement on the drainage phase diagram. The variables studied are GDL thickness, PTFE/Nafion content within the GDL, GDL compression, the inclusion of a microporous layer (MPL), and different water flow rates through the GDL. The liquid water breakthrough pressure is observed to increase with GDL thickness, GDL compression, and inclusion of the MPL. Furthermore, it has been observed that applying some amount of PTFE to an untreated GDL increases the breakthrough pressure but increasing the amount of PTFE content within the GDL shows minimal impact on the breakthrough pressure. For instance, the mean breakthrough pressures that have been measured for TGP-060 and for untreated (0 wt.% PTFE), 10 wt.% PTFE, and 27 wt.% PTFE were 3589 Pa, 5108 Pa, and 5284 Pa, respectively.

Introduction

Proton exchange membrane (PEM) fuel cells have gained much attention over the last few decades as a promising power source for automotive, portable, and stationary applications [1]. As a PEM fuel cell operates, hydrogen is oxidized in the anode and oxygen is reduced in the cathode to produce electricity, the intended product, with water and heat as byproducts. While some amount of the produced water can enhance the performance of the cell by hydrating its membrane, an excess amount of liquid water can threaten a continuous performance of the cell by filling the open pores of the gas diffusion layer (GDL). The GDL serves different roles in a PEM fuel cell. It enhances electrical contacts between the catalyst layer and the bipolar plate, supports the thin and fragile electrolyte membrane from mechanical damage, diffuses reactants over the catalyst layer, and facilitates water transport from the catalyst layer to the gas channel. Saturation of the GDL pores with liquid water is referred to as GDL flooding. GDL flooding blocks the transport of the reactants to the catalyst layer and lowers the performance of the cell by causing reactant starvation. The accumulation of excess water within the gas channel can also deteriorate the

* *Corresponding author.*
E-mail addresses: mortazav@mtu.edu (M. Mortazavi), ktajiri@mtu.edu (K. Tajiri).
http://dx.doi.org/10.1016/j.ijhydene.2014.03.238

performance of the cell by narrowing the flow cross-sectional area within the flow channel. This phenomenon is referred to as gas channel flooding and similar to GDL flooding, it can substantially deteriorate the performance of the cell. A steady performance of the cell relies on an appropriate balance between the water produced and water removed from the catalyst layer. This can be achieved by acquiring an accurate insight into the water transport phenomena across the electrode and GDL. Some studies reviewed water transport in PEM fuel cell and its balance within the membrane [2,3]. Water transport on the surface of the GDL has been previously studied by many researchers, including Mortazavi and Tajiri [4]. The current work focuses on the liquid water transport through the porous GDL.

Water transport through the porous media in fuel cells has been studied in some works. Different models have been proposed to describe the microscale liquid water transport through the GDL and micro-porous layer (MPL). Nam and Kaviany [5] studied the distribution of condensed water within the GDL and suggested that the liquid water transports from the catalyst layer to the gas channel in a branching-type geometry. According to their model, water transports through the GDL via capillary motion in a large main stream that is extended from the catalyst layer to the gas channel. The main water path is fed by smaller streams of liquid water that transport condensed micro-droplets to macro-droplets. This model has been confirmed by Pasaogullari and Wang [6] when they took a one-dimensional analytical solution of water transport phenomena within the GDL. Park et al. [7] argued that liquid shear force and water evaporation are the dominant driving forces that transport liquid water within the GDL. Litster et al. [8] suggested that the water transport through the GDL occurs by fingering and channeling. According to their hypothesis, water recedes when a dead end occurs and flows into adjacent breakthrough channels.

Similar to the GDL, water transport through the MPL has been speculated with a wide variety of hypotheses. While some studies conclude that coating a GDL with an MPL facilitates water transport from the catalyst layer to the GDL because of the pore size gradient [5,9,10], a completely opposite conclusion can also be found in literature [7]. Similarly, while some studies report that the cathode MPL enhances the back diffusion of water from the cathode to anode [11–13], others argue that the MPL has no particular impact on the back diffusion of water [14–17]. Lu et al. [18] studied liquid water transport through GDLs with and without MPL. They injected liquid water to the surface of the GDLs (MPL side for GDLs with MPL) and visualized water breakthrough from the surface of the GDLs. It has been reported that the water saturation of GDLs with MPL was lower than the water saturation of GDLs without MPL. Furthermore, they reported that for GDLs without MPL, water breakthrough locations changed dynamically but for GDLs with MPL, the breakthrough locations did not change over time. They suggested that MPL has two roles in water transport through the GDL. First, it limits the number of water entry locations into the GDL and second, it stabilized the water path through the GDL.

These controversial hypotheses emphasize the need for further studies of water transport through the GDL and MPL. A correct understanding about the liquid water transport mechanism through these components can lead to proper water removal from inside the cell. It should be added that the unique wettability and microstructural properties of each layer adds to the complication of this study.

As a common practice, GDLs are usually treated with a hydrophobic agent such as polytetrafluoroethylene (PTFE). The hydrophobic nature of the PTFE particles facilitates water removal from the GDL to the gas channel [19]. It also keeps liquid water from reentering the GDL after being expelled [8,20]. Furthermore, it has been reported that adding PTFE to GDL enhances both the gas and water transport for a cell working under flooding conditions while an excessive amount of PTFE content can lead to serious flooding in the catalyst layer [11].

Water transport through the porous structure of GDL and MPL can be studied by different approaches such as measuring the liquid water breakthrough pressure and/or visualization techniques. Bazylak comprehensively reviewed different methods of visualizing liquid water transport in PEM fuel cell components [2]. The breakthrough pressure is defined as the pressure at which liquid water passes through the porous media and emerges from the surface. The liquid water breakthrough pressure through the GDL has been measured in some studies [18,21–23]. Tamayol and Bahrami [21] measured the breakthrough pressure of 5 wt.% treated Toray carbon papers, TGP-030, TGP-060, and TGP-090. For TGP-060, they also measured the breakthrough pressure for untreated and 20 wt.% PTFE content. It has been reported that the breakthrough pressure increases with GDL thickness and PTFE content. Liu and Pan [22] analyzed water saturation inside the GDL by combining the images of water droplets on the surface of the GDL with the breakthrough pressures.

In this work, liquid water transport through the porous structure of the GDL is experimentally studied by measuring the liquid water breakthrough pressure. The liquid water breakthrough pressure is measured for different GDL thicknesses and different PTFE contents within the GDL. The effect of GDL thickness on liquid water transport through the GDL is also studied by reconstructing the pore-network of the GDL based on the GDL microstructural properties. Moreover, the effect of MPL and GDL compression on liquid water breakthrough pressure is investigated.

Experimental setup

Water breakthrough experiment

Liquid water breakthrough pressures through the GDL samples were measured with an ex-situ setup. Fig. 1 shows the schematic and the picture of the experimental setup. Water was injected to the surface of the GDL through a 250 μm diameter (Upchurch-U111) stainless steel capillary. A 1/16 inch (1.58 mm OD) FEP tube connected the stainless steel capillary to the female slip luer of the syringe in the syringe pump. The stainless steel capillary had an external diameter of 3.1 mm. The capillary was inserted into the test section via a through-all hole that was machined on one of the polycarbonate plates. The test section, made of two polycarbonate plates, held the GDL samples that were cut into pieces of

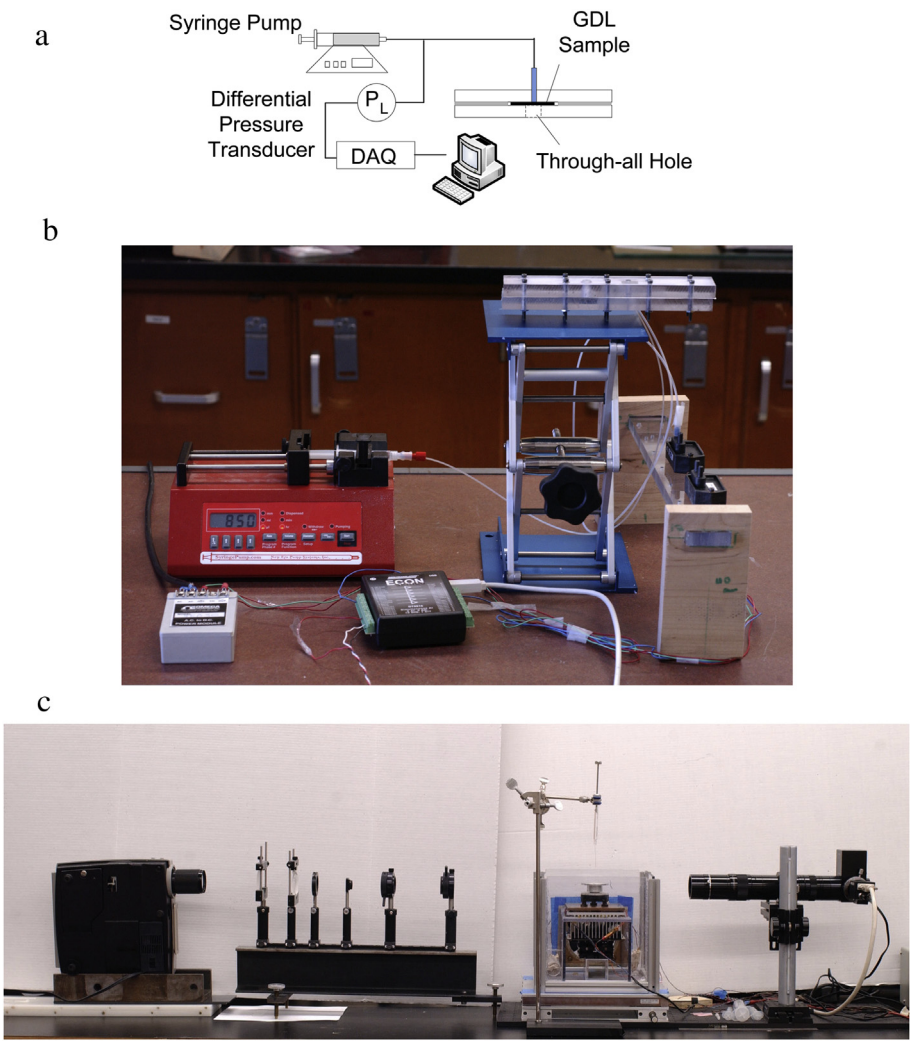

Fig. 1 – Experimental setup. (a) Schematic (b) liquid water breakthrough pressure experimental setup (c) water droplet contact angle measurement setup.

2 cm × 1 cm. A 5 mm diameter through-all hole was machined on the other polycarbonate plate (emergence side) to facilitate the water emergence. Ten 1/8 inch screws tightened the whole setup. Teflon sheets, with different thicknesses corresponding to the GDL thickness, were used to seal the whole assembly. The thicknesses of the Teflon sheets were chosen in such a way that the ratio of the GDL thickness to the Teflon sheet thickness was constant for different GDLs. A differential pressure transducer (Omega, PX163_120D5V) recorded the liquid water pressure at a sampling frequency of 50 Hz. Prior to measuring the liquid water pressure in the experiments, the pressure transducer was calibrated with a water column for accurate precision.

In general, fluid intrusion into a porous media can cause three different flow behaviors depending on the viscosity and the flow rate of the fluids involved. Fig. 2 shows these three flow regimes on a phase diagram that has been proposed by Lenormand [24,25]. This chart, which is known as the Drainage Phase Diagram, is based on two nondimensional parameters of the capillary number, *Ca*, and the viscosity ratio, *M*:

$$Ca = \frac{v\mu_{nw}}{\sigma} \tag{1}$$

$$M = \frac{\mu_{nw}}{\mu_w} \tag{2}$$

where v is the nonwetting fluid velocity, μ_w and μ_{nw} are the wetting and nonwetting fluid viscosities, and σ is the surface tension.

Viscous fingering occurs at low viscosity ratios and has been characterized as irregular conduits or fingers of the intruding fluid through the porous structure. The transition between capillary fingering to stable displacement may cause flooding, but the transition between stable displacement and viscous fingering rarely occurs in a fuel cell [26].

Table 1 lists water flow rates used in this study. It also includes the capillary number, viscosity ratio and the Reynolds number associated with each flow rate. The Reynolds number is obtained by using the superficial water velocity and a mean pore diameter of 26 μm for the GDL [27]. The superficial water velocity is defined as the bulk velocity of water passing within the capillary cross-sectional area. The low Reynolds numbers

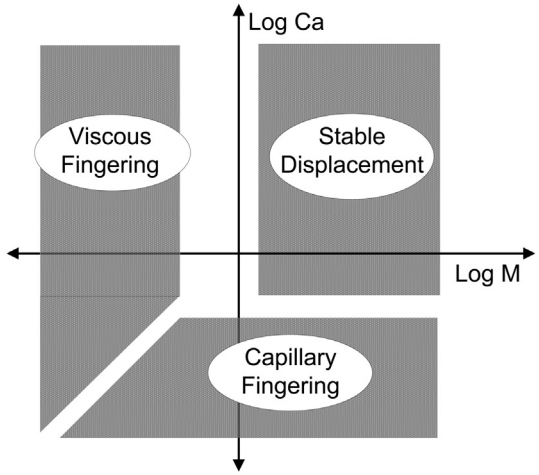

Fig. 2 – Drainage phase diagram.

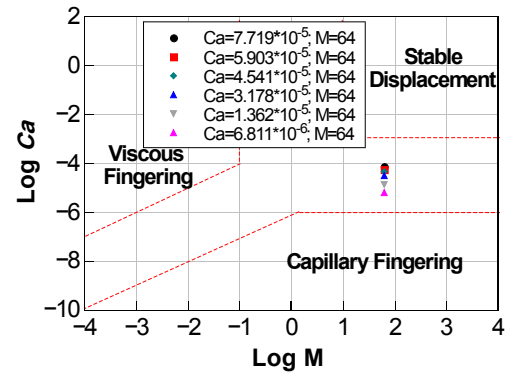

Fig. 3 – Experimental range shown on the drainage phase diagram. Dashed lines represent the hypothetical limits of flow regimes.

in Table 1 indicate that viscous effects are more dominant than inertia effects. Fig. 3 shows the range of water flow rates in the current study overlaid on the drainage phase diagram.

Sample preparation

Toray carbon papers with four different thicknesses and different PTFE contents have been used in this study. Table 2 lists the measured and calculated physical properties of GDL samples used. The carbon papers were treated with PTFE based on the procedure described in [28]. According to this procedure, the untreated carbon papers were first dipped into the PTFE emulsion (60 wt.% dispersion in H_2O, ALDRICH) for 10 h. The substrates were then put in a furnace at 120 °C for 1 h. The treating process was completed by increasing the furnace temperature to 360 °C for 1 h to make a uniform PTFE distribution through the GDL, as suggested in [28].

Contact angle measurement

Water droplet static contact angles on GDLs were measured with a house-made setup, as shown in Fig. 1(c). The procedure and theory are presented in Ref. [29]. To measure the static droplet contact angles on GDL surfaces, droplets with diameters between 1 mm to 3 mm were introduced on the GDL surface. A CCD camera (PULNIX TM-1325CL) equipped with a long distance microscope (Infinity K2/S) was used to take images of the droplets. A light source was aligned with a series of concave lenses to provide a uniform background light based on the Köhler illumination method. The images of ten droplets were captured for each GDL sample. The images were then analyzed with a computer code that was developed based on the Young–Laplace equation to give the droplet contact angles.

Table 1 – Water flow rate considered in this study.

Intruded/displaced	Water flow rate (μℓ h^{-1})	M	Ca	Re
Water/air	75	64	6.81×10^{-6}	0.0095
Water/air	150	64	1.36×10^{-5}	0.0191
Water/air	350	64	3.17×10^{-5}	0.0444
Water/air	500	64	4.54×10^{-5}	0.0635
Water/air	650	64	5.90×10^{-5}	0.0826
Water/air	850	64	7.71×10^{-5}	0.1080

Results and discussion

Contact angle

The liquid water droplet contact angle on a solid surface describes the wetting ability of the surface by liquid. The contact angle depends on the interfacial energy along the three phase boundary.

Fig. 4 shows the contact angles measured on different GDL samples. It can be observed from the figure that the contact angle remarkably changes by applying some amount of PTFE to an untreated GDL. However, the contact angle seems to be almost identical for different amounts of PTFE within the GDL. The figure also suggests that the GDL thickness does not have any particular impact on the droplet contact angle. This is in agreement with the findings reported by Whitesides and Laibinis that the droplet behavior on a solid surface is mostly governed by the wetting properties of the top few monolayers [30].

Liquid water breakthrough pressure

Liquid water can pass through the GDL pores when its pressure exceeds the capillary pressure of the GDL [5]. This capillary pressure is a function of pore size and can be described by the Young–Laplace equation:

$$P_c = P_g - P_l = \frac{2\sigma_{water}\cos\theta}{r_{pore}} \quad (3)$$

where P_g and P_l are the gas and liquid phase pressure, respectively, σ_{water} is the water surface tension, r_{pore} is the pore radius, and θ is the water contact angle on the GDL.

In an operating fuel cell, water is produced in the catalyst layer and accumulates behind the GDL. Water accumulation is

Table 2 – Properties of GDL samples.

Toray carbon paper type	Manufacturer specified thickness (μm)	Teflon sheet thickness (μm)	GDL areal mass (mg cm^{-2})	Nominal teflon loading wt.%
TGP-030	110	50	4.7 ± 0.05	0,10 ± 0.9,25 ± 2,37 ± 3.1,50 ± 4.1wt.%
TGP-060	190	80	8.6 ± 0.08	0,10 ± 0.9,25 ± 2,35 ± 3,55 ± 4.3wt.%
TGP-090	280	130	12.6 ± 0.1	0,10 ± 0.9,15 ± 1.3,35 ± 3,45 ± 3.8wt.%
TGP-120	370	130 + 50	16.5 ± 0.2	0,10 ± 1,15 ± 1.2,30 ± 3.4wt.%

accompanied with a pressure increase until its pressure reaches the capillary pressure of the GDL. At this pressure, water can intrude into the GDL, but it still needs to have a pressure greater than the GDL capillary pressure to be able to travel through the GDL. For water pressure greater than the GDL capillary pressure, the water flow rate through the GDL can be calculated based on Darcy's law:

$$Q = \frac{kA}{\mu}\frac{\Delta P}{\delta} \tag{4}$$

where Q is the water flow rate, k is the permeability, A is the cross-sectional area of the flow, ΔP is the pressure drop through the porous media, μ is the water viscosity, and δ is the length that water transports through the GDL.

Fig. 5 shows a liquid water pressure profile during the water injection at 500 μℓ/h to the surface of a 10 wt.% PTFE treated TGP-120 sample. The figure shows that the pressure increases linearly since the water injection has initiated at point A. The pressure increases until it reaches 5300 Pa at point B and then slightly drops down to the value of point C. It is speculated that the pressure increase from point A to point B corresponds to water compression behind the GDL, within the capillary tube. It is also speculated that liquid water initially penetrates into the front pores of the GDL. However, low water flow rates and small length scales involved result in low Reynolds numbers. This makes viscous damping significant and meniscus does not continuously transport within the GDL [26]. Consequently, pressure increases from point C up to point D where the pressure reaches the maximum value of 6270 Pa. At this pressure, water was observed to emerge from the surface of the GDL and form a droplet on its surface. This peak pressure is referred to as the breakthrough pressure. The droplet emergence was followed with an immediate pressure drop to 4600 Pa at point E. Fig. 5 shows that the pressure does not drop into its initial value as it had at the beginning of the experiment. This may be due to the portion of the liquid water that has not been emerged. The remaining liquid water in the GDL forms columns with the water on the surface of the GDL [31]. This causes a perpetual liquid water pressure even after droplet emergence from the surface.

The pressure profile has been further investigated by linear fitting between the points marked on the figure. The calculated slopes and their corresponding coefficient of determination, R^2, are given in Table 3. The negative slope between points B and C may reflect an initial liquid water intrusion into the GDL. Furthermore, the increasing pressure slope between intervals C-D, E-F, and G-H may indicate an increasing GDL saturation over the time. This can lead to saturation of the GDL during the operation of a PEM fuel cell that ultimately ceases its performance.

Effect of GDL thickness on the breakthrough pressure

GDL thickness has been reported to directly affect the overall performance of PEM fuel cells [11,32]. It also affects the water balance during the operation of the cell [33]. Many efforts have been done to model liquid water transport through the porous structure of the GDL. In an early study, Benziger et al. [34] proposed that GDL can be modeled as a single layer of parallel microchannels that have different diameters. According to this model, water transports through the largest pore and with minimal pressure. This model also argues that a hydrophilic GDL makes no resistance to the liquid flow and any applied pressure can drive the liquid through the GDL. According to this model, the GDL thickness has no impact on the breakthrough pressure.

GDL can also be modeled as a network of non-uniformly distributed pores that are connected by throats [35,36,21]. In this method, referred to as the pore-network model, it is assumed that the liquid and gas phases are stored in the pores and the volume occupied by throats is zero. Pores are assumed

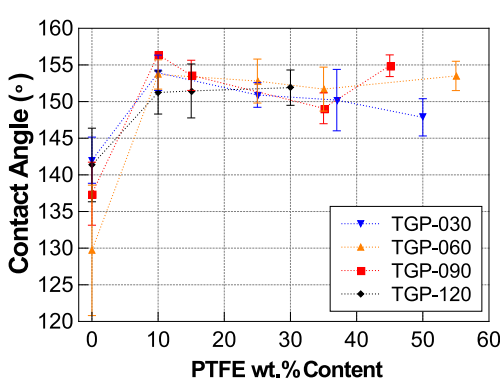

Fig. 4 – Droplets contact angles on GDL samples.

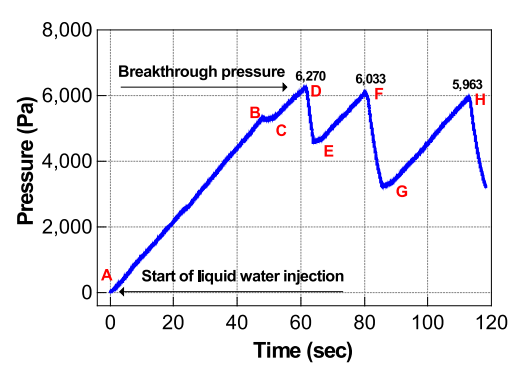

Fig. 5 – Liquid water pressure profile, water flow rate 500 μl h^{-1}, TGP-120, 10 wt.% PTFE.

Table 3 – Linear fitting of the pressure profile between points marked on Fig. 5, Pressure = $a \times$ time + b

Interval	Slope (a) (Pa s^{-1})	Intercept (b) (Pa)	R^2
A–B	111.05	−42.91	0.9997
B–C	−12.74	5912.97	0.19
C–D	92.8	551.03	0.9964
E–F	102.15	−2111.53	0.9983
G–H	108.69	−6298.9	0.9991

to have no resistance to the flow while throats resist the liquid water transport. This model suggests that the GDL thickness affects the breakthrough pressure.

In the current study, the liquid water breakthrough pressure is measured for GDLs with different thicknesses. Fig. 6 shows the measured breakthrough pressure for untreated and Nafion loaded GDLs. The results for Nafion loaded GDLs will be discussed in Section 3.2.2. Each data point on this figure represents the mean value of three replicates and the error bars represent the calculated standard deviation. The breakthrough pressure for the untreated GDL is linearly fitted and is shown with a black line on the plot. It can be observed from the figure that the breakthrough pressure increases with the GDL thickness. This is because liquid water has to pass through a longer path in thicker GDLs.

The water transport path through the GDL can be modeled by reconstructing a pore-network of GDL. Mortazavi and Tajiri [27] studied GDL microstructural properties by analyzing SEM images of Toray carbon papers. Microstructural properties such as GDL mean pore size and pore diameter distribution have been obtained in their work. In the current study, the pore diameter distribution that has been reported in Ref. [27] is utilized to investigate the effect of GDL thickness on liquid water transport through the GDL. Liquid water follows a path with minimum capillary pressure through the GDL. This path corresponds to the largest adjacent pores that are connected by throats. To investigate the effect of GDL thickness on liquid water transport through the GDL, a random matrix that describes the random distribution of GDL pores was generated. Each array was then compared to the pore size distribution to built the matrix of GDL pore diameters. The water transport path through the GDL was defined by choosing a route that has the largest adjacent pores in the matrix. In each route, the smallest pore defines the maximum pressure that liquid water needs to have to be able to pass through the GDL. Fig. 7 shows the smallest pore diameter in the water transport path through the GDL. It can be observed from the figure that the minimum pore diameter in water transport path decreases as the GDL thickness increases. This can be justified by the direct relationship between the GDL thickness and the number of pores that liquid water needs to pass, as shown in the inset of Fig. 7. As GDL thickness increases, liquid water needs to pass through a greater number of pores to be able to reach the other side of the GDL. Therefore, the possibility of having smaller pores within the water transport path increases.

It can be concluded from this figure that an increased GDL thickness has a two-fold impact on the liquid water breakthrough pressure. First, it increases the number of pores that liquid water needs to move through the GDL. Second, an increased number of pores in a thicker GDL makes the encounter of smaller pores within the water path more probable. Both of these cause an increased breakthrough pressure in thicker GDLs.

Effect of PTFE/Nafion content on the breakthrough pressure

Many works have studied the effect of the PTFE content within the GDL on the overall performance of the cell [7,11,37–40]. The common conclusion drawn from all these works suggests that the cell performance improves by adding some amount of PTFE to a raw GDL. The effect of the PTFE content on liquid water transport through the GDL has been also studied in some works [12,41,42]. However, no common conclusion about the role of PTFE on this transport phenomenon has been obtained. While some studies conclude that water transport through the GDL decreases as the PTFE content within the GDL increases [7,43], other studies confirm that the wetting characteristic of an untreated GDL only changes with some slight amount of PTFE [19,44]. These studies conclude that the wetting characteristic of GDLs are almost similar for different amounts of PTFE contents.

The effect of the PTFE content within the GDL on the liquid water breakthrough pressure is studied in the current work with the results shown in Fig. 8. Each data point is the mean value of three replicates and the error bars represent the corresponding standard deviation. The figure shows that the

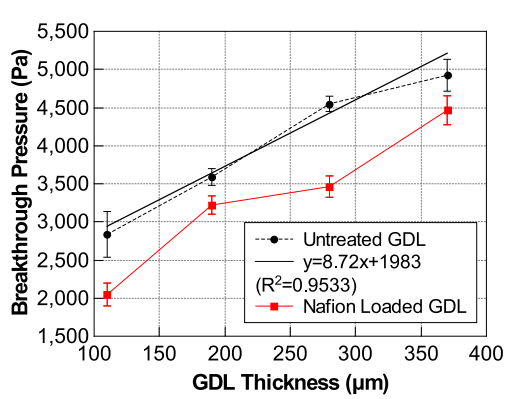

Fig. 6 – Liquid water breakthrough pressure for untreated and Nafion loaded GDLs. Water flow rate was 500 μl h^{-1}.

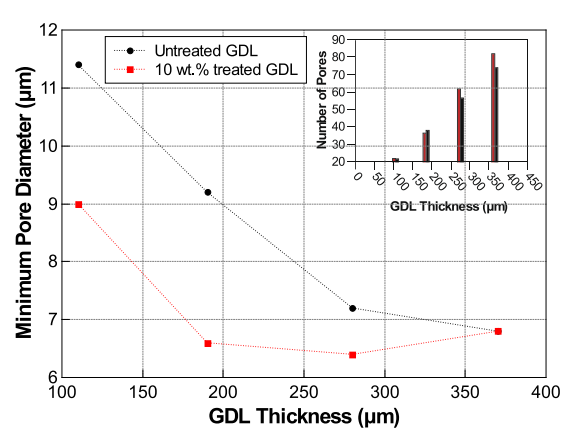

Fig. 7 – Minimum pore diameter calculated with reconstructed pore-network of GDL. GDL pore diameter distribution reported in Ref. [27] has been utilized.

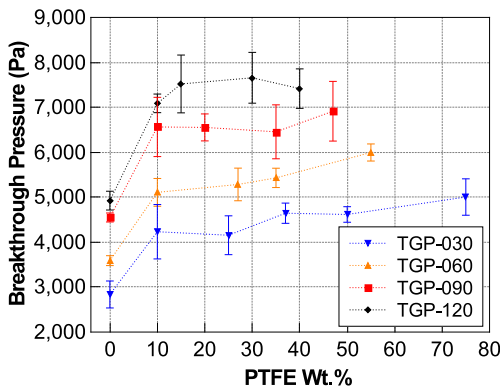

Fig. 8 – Breakthrough pressure measured for different GDLs.

breakthrough pressure significantly increases with the first addition of PTFE to an untreated GDL. However, the breakthrough pressure is observed to have minimal variation for higher amounts of PTFE. A similar trend was observed for contact angle variation shown in Fig. 4. Such observations can be interpreted as the PTFE agglomeration having only limited effects on static and dynamic behavior of liquid water within the GDL. The limited effect of the PTFE content on liquid water behavior can be explained with the heterogeneous distribution of PTFE particles through the GDL. Rofaiel et al. [45] studied heterogeneous through-plane PTFE distribution in GDLs by using SEM energy dispersive X-ray spectrometry (EDS) and noticed that for carbon paper GDLs, PTFE particles mostly concentrate within the GDL and near the two surfaces. This causes a limited concentration of PTFE particles on the GDL surface with minimal impact on the contact angle for higher amounts of PTFE content.

Fig. 9 shows the ratio of the breakthrough pressure of PTFE treated GDLs (P_b) to the breakthrough pressure of untreated GDLs ($P_{(0)}$). The figure also includes the pressure ratios reported by Benziger et al. [34] and Tamayol and Bahrami [21]. Tamayol and Bahrami [21] proposed the following pressure ratio correlation:

$$\frac{P_b}{P_{(0)}} = -0.38e^{-0.105w} + 1.38 \quad (5)$$

where w is the PTFE content in the GDL.

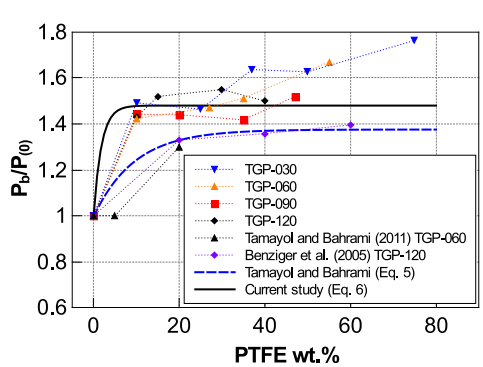

Fig. 9 – The ratio of the breakthrough pressure of treated GDLs (P_b) to the breakthrough pressure of untreated GDL (P_0). Water flow rate was 500 μl h^{-1}. The plot also includes the results presented in [34,21].

It can be observed from Fig. 9 that the correlation given in Eqn. (5) does not properly match with the findings of the current study. Therefore, a new correlation was developed that can better describe the pressure ratios obtained in this study:

$$\frac{P_b}{P_{(0)}} = -0.48e^{-0.55w} + 1.48 \quad (6)$$

Liquid water behavior through hydrophilic GDL is also interesting. Therefore, static and dynamic behavior of water within hydrophilic GDL is investigated in the current work. The hydrophilic GDL was obtained by treating GDL with Nafion. It has been reported that Nafion films are initially hydrophobic but show hydrophilic behavior as they absorb water [46]. GDLs were loaded with Nafion based on the procedure described for PTFE loading in Section 2.2. Therefore, it is expected that Nafion particles penetrate into the GDL substrate and also form a layer on its surface. In this study, 17 wt.% Nafion loaded GDL was used as a hydrophilic GDL.

Static contact angle measurements revealed a contact angle of 145°±3° for Nafion loaded GDLs. This contact angle was slightly greater than those droplet contact angles that have been measured on untreated GDLs. The contact angle observation in the current study can be justified by the hydrophobic nature of the Nafion film that covers the surface of the GDL. In the contact angle measurement experiment, water droplets were introduced to the surface of the sample. The droplets pinned to the GDL surface without being absorbed into it. Therefore, Nafion film showed its hydrophobic characteristic and the contact angle became greater than those angles that have been measured for untreated GDL.

The breakthrough pressure measured for Nafion loaded GDLs are shown in Fig. 6. It can be observed that treating GDLs with Nafion decreases the breakthrough pressure compared to untreated GDLs. This can be explained by the hydrophilic characteristic of Nafion particles as they absorb water during the water injection process. The hydrophilic property of the GDL facilitates water transport through the GDL. Therefore, droplets can emerge at lower pressures compared to untreated GDLs.

Effect of GDL compression on the breakthrough pressure

GDL compression is an important design parameter that can directly affect the performance of the fuel cell [47]. It has been reported that the GDL porosity and permeability decreases by increasing the GDL compression [48,49]. The GDL compression is therefore considered to impact the liquid water transport through the porous GDL. Bazylak et al. [50] used fluorescence microscopy to study water path through the GDL and observed that liquid water tends to flow into the compressed regions of the GDL under the land. It was reported that the compressed regions of the GDL provide preferential pathways of water transport and breakthrough. Such preferential pathways and breakthrough locations correspond to the breakup of fibers and deterioration of the hydrophobic coating.

In this study, liquid water breakthrough pressure for GDLs at different compressions have been measured for TGP-090. Different GDL compressions were achieved by using Teflon sheets with different thicknesses of 50 μm, 80 μm, 130 μm and 270 μm around the GDL sample. It was assumed that Teflon

Table 4 – Breakthrough pressure for different GDL compressions. Water was injected at 500 μℓ h^{-1}. GDL becomes more compressed as normalized GDL thickness decreases.

Toray carbon paper type	GDL thickness (μm)	Teflon sheet thickness (μm)	Normalized GDL thickness	Breakthrough pressure (Pa)
TGP-090	280	50	0.18	4481 ± 24
TGP-090	280	80	0.29	4395 ± 24
TGP-090	280	130	0.46	4239 ± 73
TGP-090	280	270	0.96	3670

sheets do not deform across their plane and the GDL thickness after compression becomes equal to the thickness of the Teflon sheet. Table 4 lists the measured breakthrough pressure for different normalized GDL thicknesses. The normalized GDL thickness was defined as:

$$\text{Normalized GDL thickness} = \frac{\text{GDL thickness after compression}}{\text{GDL thickness before compression}} \quad (7)$$

The GDL compression increases as the normalized GDL thickness decreases. Table 4 shows that the liquid water breakthrough pressure increases as GDLs become more compressed. This originates from decreased GDL porosity in higher compressions [49]. Except for the normalized thickness of 0.96 that corresponds to the thickest Teflon sheet, the other three data points represent the mean value of two replicates with uncertainties showing the standard deviation. For normalized GDL thickness of 0.96, droplet emergence was observed only in one run out of five total tests. Instead, water was observed to spread on the back side of the GDL without being emerged from the GDL surface in the other four runs. This observation suggests that a minimal GDL compression is desirable to facilitate water breakthrough.

Effect of MPL on the breakthrough pressure

GDLs are usually coated with MPLs for an improved cell performance at high current densities [37,51–53]. MPLs are known to have significant effect on water balance within the cell, because they are in direct contact with the catalyst layer. In this study, liquid water breakthrough pressure of MPL coated GDLs is measured for different water flow rates. MPL coated GDLs with the GDL substrate of TGP-060 were used in two different configurations. In one configuration, the samples were used with the MPL side in contact with the water injection capillary. Water was introduced to the surface of the MPL and its emergence from the surface of the GDL was studied. In the other configuration, the samples were put in the opposite direction with water being introduced to the surface of the GDL. Although the latter configuration is not the case for PEM fuel cells, the breakthrough pressure results can be used to characterize water transport in the electrode of unitized regenerative fuel cells. This type of fuel cells combines the functionality of a fuel cell and an electrolyzer [28].

Fig. 10 shows the measured breakthrough pressures for both of the configurations described previously. The figure also shows the breakthrough pressure for 7 wt.% PTFE and untreated GDL. Each data point is the mean value of three replicates and the error bars represent the calculated standard deviation. The figure shows that the breakthrough pressure for the MPL coated GDL is greater than that for the GDL without MPL. This is because MPL acts as an additional barrier that resists water transport through the whole media. The other observation of this figure suggests that the breakthrough pressure of MPL coated GDLs depends on the configuration of MPL and GDL. The water breakthrough from the GDL surface is observed to occur at a higher pressure rather than the water breakthrough from the MPL surface.

To further investigate the effect of MPL/GDL configuration on liquid water transport, liquid water pressure profiles for both configurations were studied, as shown in Fig. 11. It can be observed from the figure that water pressure monotonically increases when water is being injected to the surface of the MPL. However, the pressure profile for the other MPL/GDL configuration shows a small pressure drop 22 s after the initiation of water injection. This small pressure drop splits the pressure profile into two separate steps. It is speculated that each step corresponds to the water transport in either layer of GDL or MPL. The first step, with the pressure increasing up to

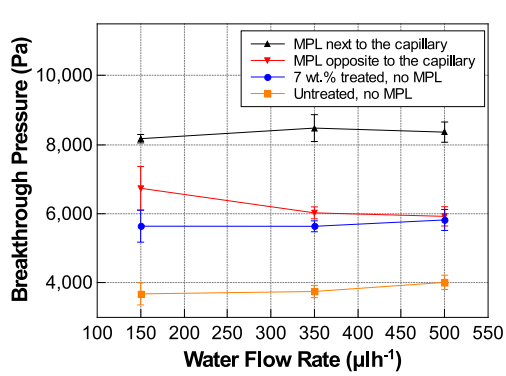

Fig. 10 – Water breakthrough pressure for different GDLs, GDL substrate TGP-060.

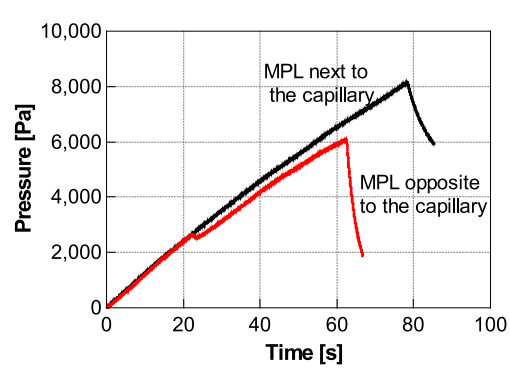

Fig. 11 – Comparison of pressure profiles for different MPL/GDL configurations at 500 μl h^{-1} water flow rate.

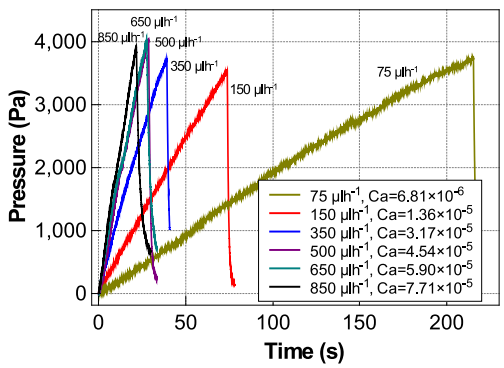

Fig. 12 – Liquid water pressure profile for different water flow rates, GDL sample untreated TGP-060.

2700 Pa, represents water transport through the GDL. Similarly, the second step, with the pressure increasing from 2700 Pa to 6100 Pa, represents water transport through the MPL.

Effect of water flow rate on the breakthrough pressure

The liquid water breakthrough pressures that have been presented until now have been obtained at water flow rate of 500 μℓ/hthat corresponds to the capillary number 4.54×10^{-5}. Because flow behavior in porous media depends on the capillary number, which itself is a function of fluid velocity (Equation (1)), it may be assumed that the breakthrough pressure varies with the water flow rate. Therefore, the effect of the water flow rate on the breakthrough pressure has been studied by injecting water at different flow rates between 75 μℓ/hand 850 μℓ/h. Such flow rates correspond to capillary numbers $6.81 \times 10^{-6}$and 7.71×10^{-5}, respectively. Fig. 12 shows the pressure profiles that have been recorded at different water flow rates. It can be observed from the figure that the breakthrough pressure shows minimal variation with water flow rate. However, water flow rate affects the pressure profile slope and the time interval that water needs to travel through the GDL to emerge from its surface. A higher water flow rate provides a higher superficial water velocity through the GDL and decreases water transport time through the GDL.

Fig. 12 also shows that the pressure profile oscillates with a greater amplitude at lower capillary numbers. This increased oscillatory pattern of the pressure profile at lower capillary numbers originates from the low flow rate that is not capable of providing enough volume of water to keep a continuous meniscus transport [26]. Therefore, water percolation through the GDL subsides. Water accumulates until the pressure exceeds the capillary pressure of the pore and can pass through the pore. As the capillary number increases, the flow regime shifts to the stable displacement and pressure oscillation decreases.

Conclusion

Liquid water transport through the porous structure of the GDL was studied by measuring the liquid water breakthrough pressure with an ex-situ approach. Toray carbon papers with different thicknesses and different PTFE contents were used as GDLs. The breakthrough pressures have been also measured for different GDL compressions. The effect of MPL on the breakthrough pressure has been studied as well. GDL pore size distribution reported in Ref. [27] were utilized to reconstruct the pore-network of GDL. The following conclusions can be drawn from this study:

1. GDL thickness does not affect the droplet contact angle. For treated Toray carbon papers with different thicknesses, a contact angle with a mean value of ~152°has been obtained. Measuring similar contact angles for different GDL thicknesses is because the droplet behavior on a solid surface is mostly governed by the wetting properties of the top few monolayers.
2. The liquid water breakthrough pressure increases with GDL thickness. For untreated Toray carbon papers with 110 μm, 190 μm, 280 μm, and 370 μm thicknesses, the mean value of the measured breakthrough pressures were 2836 Pa, 3589 Pa, 4549 Pa, and 4924 Pa, respectively (Fig. 8). GDL thickness can be mentioned to have a two-fold impact on the liquid water breakthrough pressure. First, it increases the number of pores liquid water needs to pass through the GDL to emerge from its surface. The greater number of pores, consequently, increases the probability of having smaller pores within the water transport path (Fig. 7).
3. Applying some amount of PTFE to an untreated GDL increases the breakthrough pressure. However, the breakthrough pressure does not vary with different amounts of the PTFE within the GDL. For instance, for untreated TGP-060, 10 wt.% PTFE treated TGP-060, and 27 wt.% PTFE treated TGP-060, the measured breakthrough pressures were 3589 Pa, 5108 Pa, and 5284 Pa, respectively (Fig. 8).
4. It was observed that treating a GDL with Nafion increases the droplet contact angle compared to an untreated GDL. However, Nafion treatment of GDLs was observed to decrease the water breakthrough pressure. Such observations were justified according to the different characteristics of Nafion film for dry and wet conditions.
5. GDL compression was observed to increase the breakthrough pressure. This is because GDL porosity decreases as the GDL becomes more compressed.
6. The MPL coating of GDLs were observed to increase the liquid water breakthrough pressure through the GDL. At water flow rate of 150 μℓ h^{-1}, the breakthrough pressure for TGP-060 without MPL was 5640 Pa while the breakthrough pressure for the same substrate with MPL was 8175 Pa (Fig. 10). It was also observed that different configurations of MPL and GDL result in different breakthrough pressures. The breakthrough pressure when MPL was in contact with the capillary tube was greater than the breakthrough pressure when GDL was in contact with the capillary tube.

It should be added that while these results are obtained based on an ex-situ approach, they can still be utilized in a successful PEM fuel cell design. The increased breakthrough pressure for thicker GDLs, for instance, is a design parameter that should be carefully considered in a PEM fuel cell design. Similarly, the lower breakthrough pressure for lower GDL compression may be considered as a potential remedy for an improved water management in PEM fuel cells.

Acknowledgment

Michigan Technological University is gratefully acknowledged for providing the startup fund for this study. The authors would like to thank Vinaykumar Konduru from Microfluidic and Interfacial Transport Laboratory [35] at Michigan Technological University for measuring the contact angles of droplets on GDLs.

REFERENCES

[1] Faghri A, Guo Z. Challenges and opportunities of thermal management issues related to fuel cell technology and modeling. Int J Heat Mass Transf 2005;48(19):3891–920.
[2] Bazylak A. Liquid water visualization in PEM fuel cells: a review. Int J Hydrogen Energy 2009;34(9):3845–57.
[3] Dai W, Wang H, Yuan ZZ, Martin JJ, Yang D, Qiao J, Ma J. A review on water balance in the membrane electrode assembly of proton exchange membrane fuel cells. Int J Hydrogen Energy 2009;34(23):9461–78.
[4] Mortazavi M, Tajiri K. Effect of the PTFE content in the gas diffusion layer on water transport in polymer electrolyte fuel cells (PEFCs). J Power Sources 2014;245:236–44.
[5] Nam JH, Kaviany M. Effective diffusivity and water-saturation distribution in single-and two-layer PEMFC diffusion medium. Int J Heat Mass Trans 2003;46(24):4595–611.
[6] Pasaogullari U, Wang CY. Liquid water transport in Gas diffusion layer of polymer electrolyte fuel cells. J Electrochem Soc 2004;151:A399–406.
[7] Park GG, Sohn YJ, Yang TH, Yoon YG, Lee WY, Kim CS. Effect of PTFE contents in the gas diffusion media on the performance of PEMFC. J Power Sources 2004;131:182–7.
[8] Litster S, Sinton D, Djilali N. Ex situ visualization of liquid water transport in PEM fuel cell gas diffusion layers. J Power Sources 2006;154(1):95–105.
[9] Pasaogullari U, Wang CY, Chen KS. Two-phase transport in polymer electrolyte fuel cells with bilayer cathode gas diffusion media. J Electrochem. Soc 2005;152(8):A1574–82.
[10] Pasaogullari U, Wang CY. Two-phase transport and the role of micro-porous layer in polymer electrolyte fuel cells. Electrochim Acta 2004;49(25):4359–69.
[11] Lin G, Nguyen TV. Effect of thickness and hydrophobic polymer content of the Gas diffusion layer on electrode flooding level in a PEMFC. J Electrochem Soc 2005;152:A1942–8.
[12] Spernjak D, Prasad AK, Advani SG. Experimental investigation of liquid water formation and transport in a transparent single-serpentine PEM fuel cell. J Power Sources 2007;170:334–44.
[13] Weber A, Newman J. Effects of microporous layers in polymer electrolyte fuel cells. J Electrochem Soc 2005;152:A677–88.
[14] Pharoah JG, Peppley B, Atiyeh H, Halliop E, Karan K, Phoenix A. Investigating the role of a microporous layer on the water transport and performance of a PEMFC. ECS Trans 2006;3(1):1227–37.
[15] Karan K, Atiyeh H, Phoenix A, Halliop E, Pharoah J, Peppley B. An experimental investigation of water transport in PEMFCS. Electrochem Solid-State Lett 2007;10:B34.
[16] Atiyeh H, Karan K, Peppley B, Phoenix A, Halliop E, Pharoah J. Experimental investigation of the role of a microporous layer on the water transport and performance of a PEM fuel cell. J Power Sources 2007;170(1):111–21.
[17] Malevich D, Halliop E, Peppley BA, Pharoah JG, Karan K. Investigation of charge-transfer and mass-transport resistances in PEMFCS with microporous layer using electrochemical impedance spectroscopy. J Electrochem Soc 2009;156(2):B216–24.
[18] Lu Z, Daino MM, Rath C, Kandlikar SG. Water management studies in PEM fuel cells, part III: dynamic breakthrough and intermittent drainage characteristics from GDLs with and without MPLs. Int J Hydrogen Energy 2010;35(9):4222–33. http://dx.doi.org/10.1016/j.ijhydene.2010.01.012.
[19] Fairweather JD, Cheung P, Schwartz DT. The effects of wetproofing on the capillary properties of proton exchange membrane fuel cell gas diffusion layers. J Power Sources 2010;195(3):787–93.
[20] Li H, Tang Y, Wang Z, Shi Z, Wu S, Song D, et al. A review of water flooding issues in the proton exchange membrane fuel cell. J Power Sources 2008;178(1):103–17.
[21] Tamayol A, Bahrami M. Water permeation through gas diffusion layers of proton exchange membrane fuel cells. J Power Sources; 2011:6356–61.
[22] Liu TL, Pan C. Visualization and back pressure analysis of water transport through gas diffusion layers of proton exchange membrane fuel cell. J Power Sources 2012;207.
[23] Kandlikar SG, Garofalo ML, Lu Z. Water management in a PEMFC: water transport mechanism and material degradation in gas diffusion layers. Fuel Cells 2011;11:814–23.
[24] Lenormand R, Touboul E, Zarcone C. Numerical models and experiments on immiscible displacements in porous media. J Fluid Mech 1988;189:165–87.
[25] Lenormand R. Liquids in porous media. J Phys-Condens Mat 1990;2:SA79–311.
[26] Medici E, Allen J. Existence of the phase drainage diagram in proton exchange membrane fuel cell fibrous diffusion media. J Power Sources 2009;191(2):417–27.
[27] Mortazavi M, Tajiri K. In-plane microstructure of gas diffusion layers with different properties for PEFC. J Fuel Cell Sci Tech 2014;11(2):021002-1–021002-9. http://dx.doi.org/10.1115/1.4025930.
[28] Hwang CM, Ishida M, Ito H, Maeda T, Nakano A, Hasegawa Y, Yokoi N, Kato A, Yoshida T. Influence of properties of gas diffusion layers on the performance of polymer electrolyte-based unitized reversible fuel cells. Int J Hydrogen Energy 2010;36:1740.
[29] Konduru V. Static and dynamic contact angle measurement on rough surfaces using sessile drop profile analysis with application to water management in low temperature fuel cells [Master's thesis]. Michigan Technological University; 2010.
[30] Whitesides GM, Laibinis PE. Wet chemical approaches to the characterization of organic surfaces: self-assembled monolayers, wetting, and the physical-organic chemistry of the solid-liquid interface. Langmuir 1990;6(1):87–96.
[31] Das PK, Grippin A, Kwong A, Weber A. Liquid-water-droplet adhesion-force measurements on fresh and aged fuel-cell gas-diffusion layers. J Electrochem. Soc 2012;159:489–96.
[32] Ihonen J, Mikkola M, Lindbergh G. Flooding of Gas diffusion backing in PEFCs, physical and electrochemical characterization. J Electrochem Soc 2004;151(8):A1152–61.
[33] Zhou Y, Jiao K, Du Q, Yin Y, Li X. Gas diffusion layer deformation and its effect on the transport characteristics and performance of proton exchange membrane fuel cell. Int J Hydrogen Energy 2013;38(29):12891–903.
[34] Benziger J, Nehlsen J, Blackwell D, Brennan T, Itescu J. Water flow in the gas diffusion layer of PEM fuel cells. J Membr Sci 2005;261(1–2):98–106.
[35] Gostick JT, Ioannidis MA, Fowler MW, Pritzker MD. Pore network modeling of fibrous gas diffusion layers for polymer

electrolyte membrane fuel cells. J Power Sources 2007; 173(1):277–90.
[36] Sinha P, Wang C. Pore-network modeling of liquid water transport in gas diffusion layer of a polymer electrolyte fuel cell. Electrochim Acta 2007;52(28):7936–45.
[37] Paganin VA, Ticianelli EA, Gonzalez ER. Development and electrochemical studies of gas diffusion electrodes for polymer electrolyte fuel cells. J Appl Electrochem 1996;26:297–304.
[38] Lim C, Wang CY. Effects of hydrophobic polymer content in GDL on power performance of a PEM fuel cell. Electrochim Acta 2004;49(24):4149–56.
[39] Song JM, Cha SY, Lee WM. Optimal composition of electrolyte fuel cell electrodes determined by the ac impedance method. J Power Sources 2001;94(1):78–84.
[40] Lobato J, Canizares P, Rodrigo MA, Ruiz-López C, Linares JJ. Influence of the teflon loading in the gas diffusion layer of PBI-based PEM fuel cells. J Appl Electrochem 2008;38(6):793–802.
[41] Tüber K, Pócza D, Hebling C. Visualization of water buildup in the cathode of a transparent PEM fuel cell. J Power Sources 2003;124(2):403–14.
[42] Ge S, Wang CY. Liquid water formation and transport in the PEFC anode. J Electrochem Soc 2007;154(10):B998–1005.
[43] Dai W, Wang H, Yuan XZ, Martin J, Shen J, Pan M, Luo Z. Measurement of water transport rates across the gas diffusion layer in a proton exchange membrane fuel cell, and the influence of polytetrafluoroethylene content and microporous layer. J Power Sources 2009;188(1):122–6.
[44] Gostick JT, Ioannidis MA, Fowler MW, Pritzker MD. Wettability and capillary behavior of fibrous gas diffusion media for polymer electrolyte membrane fuel cells. J Power Sources 2009;194(1):433–44.
[45] Rofaiel A, Ellis JS, Challa PR, Bazylak A. Heterogeneous through-plane distributions of polytetrafluoroethylene in polymer electrolyte membrane fuel cell gas diffusion layers. J Power Sources 2012;201:219–25.
[46] Li X, Feng F, Zhang K, Ye S, Kwok DY, Birss V. Wettability of Naïon and Naïon/Vulcan carbon composite films. Langmuir 2012;28:6698–705.
[47] Ge J, Higier A, Liu H. Effect of gas diffusion layer compression on PEM fuel cell performance. J Power Sources 2006;159(2):922–7.
[48] Hussaini I, Wang C. Measurement of relative permeability of fuel cell diffusion media. J Power Sources 2010;195(12):3830–40.
[49] Gostick JT, Fowler MW, Pritzker MD, Ioannidis MA, Behra LM. In-plane and through-plane gas permeability of carbon fiber electrode backing layers. J Power Sources 2006;162(1):228–38.
[50] Bazylak A, Sinton D, Liu ZS, Djilali N. Effect of compression on liquid water transport and microstructure of PEMFC gas diffusion layers. J Power Sources 2007;163(2):784–92.
[51] Qi Z, Kaufman A. Improvement of water management by a microporous sublayer for PEM fuel cells. J Power Sources 2002;109(1):38–46.
[52] Giorgi L, Antolini E, Pozio A, Passalacqua E. Influence of the PTFE content in the diffusion layer of low-Pt loading electrodes for polymer electrolyte fuel cells. Electrochim Acta 1998;43(24):3675–80.
[53] Jordan L, Shukla A, Behrsing T, Avery N, Muddle B, Forsyth M. Diffusion layer parameters influencing optimal fuel cell performance. J Power Sources 2000;86(12):250–4.